

Preparation of α -Fe₂O₃ Nano-photocatalyst supported on Cd(II)-Terephthalic MOF for photocatalytic removal of Cefazolin aqueous solution

Seyed Kamal Blourfrosh, Kazem Mahanpoor*

Department of Chemistry, Arak Branch, Islamic Azad University, Arak, Iran

Received 22 September 2020; received in revised form 8 March 2021; accepted 7 April 2021

ABSTRACT

The main purpose of this study was to investigate the photocatalytic decomposition of the antibiotic Cefazolin (CFZ) from aqueous solutions using a new effective catalyst. This catalyst was made of α -Fe₂O₃-supported nanoparticles on a metal-organic framework (MOF). The synthesis of Nano α -Fe₂O₃ photocatalyst was performed by the reflux condensation method. The MOF was synthesized using Cadmium nitrate and Terephthalic acid and Nano α -Fe₂O₃ supported on MOF using a solid-state distribution (SSD) method. FTIR, XRD, SEM, EDX, N₂ adsorption-desorption and TGA technique were used for the identification of the catalyst. Analysis of these results revealed that α -Fe₂O₃ circular nanoparticles bonded together and occupy a large area on the MOF crystal surfaces. The BET surface area and the pore diameter of the catalyst obtained were 479 m²g⁻¹ and 3.86 nm respectively. UV/H₂O₂ photocatalytic processes were applied for the decomposition of CFZ from aqueous solutions. This process was optimized and modeled using the full factorial method. Initial concentrations of CFZ, pH, α -Fe₂O₃/MOF amounts and initial concentration of H₂O₂ were the variables for the determination of optimal conditions and mathematical models. The highest degradation percentage of CFZ in the optimum condition (CFZ=30 ppm, pH=8, H₂O₂=5ppm, catalyst=150mg.l⁻¹) was 85.88%. This photocatalyst reaction has pseudo-first-order kinetic with a constant rate of 0.0752 min⁻¹ and it also matched the Langmuir–Hinshelwood model.

Keywords: Photocatalyst, Cefazolin, α -Fe₂O₃, Metal-Organic Framework, solid-state distribution

1. Introduction

Many medicinal compounds are toxic and dangerous to the environment, natural resources and humans, therefore they are new risk factors for soil and water organisms. Small amounts of antibiotic residuals always exist in the environment; they can cause antibiotic-resistant bacterial colonies and inactivate antibiotics in the near future [1]. Cephalosporin drugs are the most common antibiotic known as an emerging water pollutant. Cefazolin (CFZ) is one of the cephalosporin antibiotics used for treating urinary tract infections, cellulitis, pneumonia, endocarditis, biliary tract infections, and joint infection [2]. CFZ is water-soluble at different temperatures and various pH ranges [1-3].

In the last few years, different technologies have been evaluated for pharmaceutical compounds removal, such as membrane filtration, activated carbon adsorption and biological techniques [2, 4]. These technologies have s-

ome limitations and disadvantages such as transfer of contaminants from one phase to another, incomplete removal of contaminants, high energy consumption and production of sludge or toxic waste. Recent researches have shown that the use of heterogeneous photocatalytic processes as the most effective advanced oxidation process (AOP) does not have these disadvantages [2]. In heterogeneous photocatalysis, the light energy equal to or higher than the band gap energy of a semiconductor, produces electron-hole pairs on the catalyst surface. O₂ will absorb the photo-generated electrons to produce superoxide radical ions ([•]O_{2(ads)}⁻) and the photogenerated holes (h⁺) can oxidize H₂O or OH⁻ to yield [•]OH. These radicals can attack to pollutant molecules and convert them into CO₂ and H₂O [5].

Here are some of the researches done in this field. The BiVO₄-WO₃ Nano-composite catalyst was used in the photodegradation of Sulfasalazine (one of the disease-modifying ant rheumatic drugs) an aqueous solution.

*Corresponding author:

E-mail address: k-mahanpoor@iau-arak.ac.ir (K. Mahanpoor);

This catalyst was able to remove about 76% of Sulfasalazine as a pollutant from aqueous solution after 50 min UV irradiation [5]. Jiao et al. (2008) conducted a study on the Tetracycline – as a low sensitivity antibiotic decomposition using UV. They removed 73% of Tetracycline in 300-minute retention time [6]. Derikvandi et al. (2017) did research on the photocatalytic degradation of the Metronidazole aqueous solution as an antibiotic and antiprotozoal medication. They used a mixture of NiO and ZnO stabilized on the Clinoptilolite as a photocatalyst and were able to remove more than 87.7% of metronidazole contamination from water after 50 min UV irradiation [7]. Pourtaheri et al (2015) analyzed Cefexim antibiotic photocatalytic decomposition process using NiO/Clinoptilolite as a heterogeneous photocatalyst under Hg-lamp irradiation. They concluded that in the 300-minute retention time of process, about 80% of the primary Cefexim will be decomposed [8].

The catalysts used in heterogeneous photocatalytic processes are usually metal oxide semiconductors and play a major role in these processes. A large variety of oxides has been evaluated to remove the pollutants from aqueous solutions. Among them, α -Fe₂O₃ has been widely studied as a catalyst for various photocatalytic reactions because it is a semiconductor with an energy gap of 2.2 eV, high chemical stability, non-toxic and inexpensive [9].

A perfect run of the heterogeneous photocatalytic process by using the semiconductor as a catalyst includes the collision of the irradiated UV or visible photons, the excitation of the semiconductor to produce the electron-hole (e^-/h^+) pairs as the charge carriers, the (e^-/h^+) separation and their transference to the surface of the semiconductor and resulting in the redox reactions on its surface [5, 10].

One of the problems of semiconductor photocatalysts is that they can recombine before the photogenerated (e^-/h^+) pairs reach the surface of the semiconductor, thus consuming the energy used as heat. The recombination of (e^-/h^+) pairs reduces the efficiency of this effective method. Different methods such as the size decreasing, supporting, coupling and doping of semiconductors have been used to reduce the (e^-/h^+) recombination. In all these methods, the path length is reduced quickly to reach the (e^-/h^+) pairs at the surface of the semiconductor catalyst. On the other hand, the pollutants adsorption on the catalyst surface is closely related to the photocatalytic degradation process. If the catalyst has a high adsorption property, the contaminant molecules are placed near the active radicals on the surface of the catalyst and decompose rapidly.

Therefore, among the various methods used to reduce the (e^-/h^+) recombination composition, the catalytic supporting method would be very efficient [10].

Today, a new porous metal-organic frameworks (MOFs) has emerged, combining inorganic metal ions and multifunctional organic ligands that have many strengths including different types, adjustable structure and adjustable, low crystal density and specific surface area compared to porous molecular sieve and activated carbon [11]. Reduction of problems, including catalyst aggregation and smaller specific surface area, is beneficial due to its unique structure and MOF properties, so the photocatalysts performance in the combination with MOFs is expected to increase [11-13]. Now, this has become a research frontier and a hotspot in materials science.

The catalyst problems used in photocatalytic processes, including catalyst aggregation and smaller specific surface area, can be solved through the unique structure and properties of MOFs, so catalytic performance is expected to increase by combining MOF with photocatalyst [11-13]. In this study, the α -Fe₂O₃ photocatalyst was stabilized in MOF.

The common method for optimizing the conditions of a process or an experiment is one factor at a time (OFAT). In this method, one factor changes at any time and other factors are constant. Today, statistical methods for process optimization have been developed, known as design of experiments (DOE) methods. In DOE methods, different factors can change simultaneously [14]. DOE compared to OFAT has advantages such as 1- reducing the number of experiments and their costs; 2-determining the share of each factor in the experiment result 3- Independence of experiment results from other experiments; 4-determining the share of interaction variables in experiment results 5-possibility of estimating results under optimal conditions 6-obtaining experimental results in a wider area of the operating space. Therefore, DOE will be more efficient when two or more factors are considered in an experiment [14, 15].

In the present research, Nano α -Fe₂O₃/MOF photocatalyst was prepared and identified with proper techniques such as Ft-IR, SEM, EDX, XRD, N₂ adsorption-desorption and TGA. The photocatalytic degradation of CFZ was investigated in batch photoreactor using Nano α -Fe₂O₃/MOF photocatalysts aqueous suspension and H₂O₂. The experiments are performed using a 2⁴factorial design to investigate the main effects and the interactions between variables (pH, the initial concentration of H₂O₂, the primary concentration of CFZ and Nano α -Fe₂O₃/MOF amount).

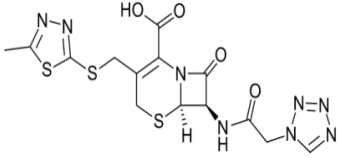
2. Experimental

2.1. Materials

All chemicals used in this work including Cadmium nitrate tetrahydrate, Terephthalic acid, Iron (III) chloride hexahydrate, Urea, Ammonium, Hydrogen peroxide (30% purity), Hydrochloric acid (37% purity),

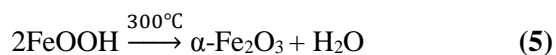
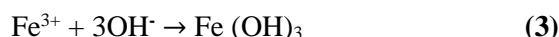
Sulfuric acid (96% purity), Sodium hydroxide, and Ethanol were purchased from Merck Company and were utilized without further purification. The required CFZ was purchased from Alborz Darou Pharmaceutical Company (Qazvin, Iran). The structure and chemical properties of CFZ are seen in **Table 1**.

Table 1. CFZ chemical properties

Empirical formula	Structural formula	IUPAC Name
C ₁₄ H ₁₄ N ₈ O ₄ S ₃ (Mw =454.51)		3- [[[(5-methyl-1,3,4-thiadiazol- (6R,7R)2-yl) thio] methyl]-8-oxo-7-[(1H-tetrazol-1-yl)acetyl] amino]-5-thia-1-azabicyclo [4.2.0] oct-2-ene-2-carboxylic acid

2.2. Preparation of α -Fe₂O₃

The synthesis of the α -Fe₂O₃ photocatalyst was carried out according to the reflux density method of Bharathi et al [16]. 4.054 g iron (III) chloride hexahydrate was dissolved in 50 ml deionized water and 100 ml urea solution (1 M) was added to this solution and was refluxed at 95 °C for 12 hours. The obtained sediment was separated by centrifugation. The precipitate was washed three times with distilled water and dried in an oven at 80 °C and it was put in a furnace at 300 °C for 4 hours. The red solid compound was cooled and rubbed in a mortar. The α -Fe₂O₃ synthesis reactions are presented in the following reactions (1-5). [16].



2.3. Synthesis of MOF

Tetra hydrate Cadmium nitrate hydrate (6.169 g) in 50 ml of deionized water and terephthalic acid (2.491 g) in 50 ml deionized water and ethanol (50% v/v) was dissolved. These two solutions were mixed and stirred for half an hour. The resultant solution was placed in an autoclave at 120 °C for 15 hours. It was cooled about ambient temperature and filtered after crystallization and washed by water and ethanol several times and placed in the oven at the temperature of 220 °C.

2.4. Stabilization of α -Fe₂O₃ on MOF

The α -Fe₂O₃ was stabilized on the MOF with solid-state dispersion (SSD) method [26]. In this method, α -Fe₂O₃ (1g) was mixed with MOF (3g) using ethanol with an agate pestle and mortar. This product was dried at 110 °C and calcined in the air at 450 °C for 5 h to get Fe₂O₃/MOF catalysts.

2.5. Apparatus

Furnace (Sef-201 Korea), oven (OF-02), and ALC4232 centrifuge were used to make the catalyst. XRF model (Nitin XL 3t), XRD model (DX-27Mini 40kV/25mA), SEM model (Philips XL-30) and FT-IR model (Perkin Elmer Spectrum 400) devices were used in the identification of the catalyst. N₂ adsorption/desorption isotherms at 77 K were measured using volumetric adsorption equipment (Bedsore-Max-S, BEL Japan Inc., Japan). The TGA device (Perkin Elmer Pyres 1, USA) was used to find the stability and thermal degradation properties of the samples. Chemical oxygen demands (COD) of samples were measured by the potassium dichromate titration method (Standard Method 5220). All Ultraviolet/Visible (UV/Vis) absorption spectra for determining COD were obtained by an Agilent 8453 spectrophotometer. Total organic carbon (TOC) of samples was measured by ANATOC™ Series II manufactured by the Australian SGE Company.

A 500 mm Pyrex reactor was located inside a 60 cm long wooden cube, and three Philips lamps (45 cm 15 watts of mercury) were mounted on top of the wooden cube. The liquid inside the reactor was continuously mixed with a magnetic stirrer. A fan was placed behind the cube to ventilate the air inside the box. The scheme of this experiment equipment is shown in **Fig. 1**.

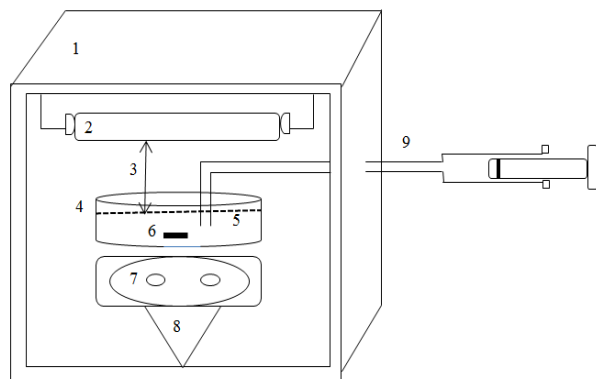


Fig. 1. Schematic of photocatalyst reactor: 1) wooden chamber with 60×60×60 cm dimensions; 2) three Philips 15 w lamps; 3) 5 cm gap between liquid surface and the lamp; 4) unbreakable container against temperature with 0.5 l capacity; 5) 250 ml antibiotic solution; 6) magnet; 7) magnetic stirrer; 8) metal foot; 9) 5 ml syringe

2.6. Procedure of photocatalytic degradation of CFZ

Full factorial designs method with a different variable containing initial concentrations of CFZ, α -Fe₂O₃/MOF amounts, initial concentration of H₂O₂ and pH (as specified in **Table 2**) was used. Sulfuric acid and sodium hydroxide solutions (0.1 mol. l⁻¹) were used to adjust pH. For the photocatalytic degradation of CFZ, a solution containing the known concentration of CFZ and photocatalyst (according to **Table 2**) was prepared and allowed to equilibrate in the dark for 30 min (to eliminate adsorption effects). Then a certain amount of hydrogen peroxide was added, and the sample was exposed to ultraviolet radiation. UV-Vis spectrophotometric method was used to measure the CFZ concentration. The maximum absorption wavelength for CFZ in aqueous solution was 270 nm.

3. Result and Discussion

3.2. Identification of Catalyst

Photocatalyst was identified with XRD, SEM, EDX, TGA, N₂ adsorption-desorption and FTIR techniques. FTIR spectroscopy was used for identification of the surface functional groups of nanoparticles. FT-IR spectra of raw α -Fe₂O₃, MOF and α -Fe₂O₃/MOF samples are shown in **Fig. 2**. According to **Fig. 2-A**, the infrared spectrum (FTIR) of the synthesized α -Fe₂O₃ nanoparticles was identified the chemical bonds as well as functional groups in the compound. The large broad band in the range 3400-3500 cm⁻¹ is ascribed to the O-H stretching vibration in OH groups. The strong band below 700 cm⁻¹ is assigned Fe-O stretching mode. The band corresponding to Fe-O stretching mode of α -Fe₂O₃ is seen at 576 cm⁻¹ [17].

In the FTIR spectroscopy of MOF (**Fig. 2-B**), stretching vibration band of O-H groups was appearing at the 3416 cm⁻¹. The vibration band of C=C and C-C related to benzene ring and C=O related to carboxylic acid in the terephthalic acid structure appeared in the range of 3400-3500 cm⁻¹. The bands at 525 and 736 cm⁻¹ are related to Cd-O vibration.

As shown in the FTIR spectrum of α -Fe₂O₃/MOF (**Fig. 2-C**), all MOF and α -Fe₂O₃ vibration modes are present at the spectra of Fe₂O₃/MOF sample, confirming that MOF and α -Fe₂O₃ structure unchanged during calcination processes.

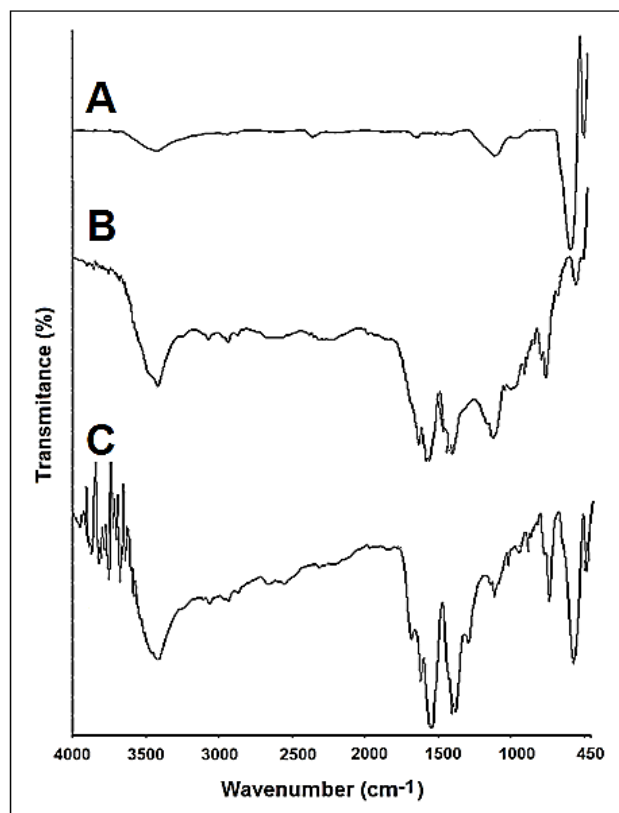


Fig. 2. FTIR spectroscopy of α -Fe₂O₃ (A), MOF(B) and α -Fe₂O₃/MOF

X-ray powder diffraction (XRD) is an analytical technique used for phase identification of a crystalline material and can provide information on unit cell dimensions. The analyzed material was finely ground, homogenized, and average bulk composition was determined. The XRD pattern of the samples is shown in **Fig 3**. The XRD pattern of the α -Fe₂O₃ sample is composed with several diffraction peaks (012), (104), (110), (113), (024), (116), (214) and (300) assigned to the diffraction planes of rhombohedra structure of α -Fe₂O₃ phase (JCPDS card No: 79-0007) [18,19]. No secondary phases were detected, indicating the purity of the synthesized powder and that is composed of α -Fe₂O₃ single phase. No diffraction peaks were observed for the

FeOOH phase, indicating that thermal annealing completely changed FeOOH to α -Fe₂O₃.

MOF peaks are shown in the XRD diffraction pattern (Fig.3-B). The position of these peaks has not changed since the α -Fe₂O₃ support on MOF. Therefore, the main structure and crystalline of MOF are stable.

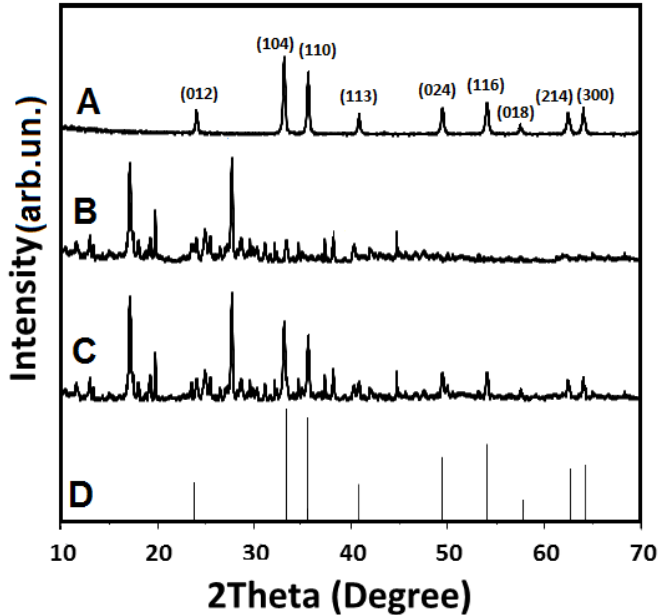


Fig. 3. XRD pattern of α -Fe₂O₃ (A), MOF (B), α -Fe₂O₃/MOF(C) and α -Fe₂O₃ phase (JCPDS card No: 79-0007) (D)

The crystallite size is calculated by using Debye-Scherrer method [20, 21], which is given by the Eq. (1).

$$D = \frac{k\lambda}{\beta \cos\theta} \quad (\text{Eq.1})$$

where, D is the crystallite size in nm scale, K is shape factor which is equal to 0.9, λ is the wavelength of X-ray radiation ($\lambda = 1.5406 \text{ \AA}$), β is the full width half maximum intensity (FWHM) and θ is the Bragg's angle.

The crystal size was calculated using the Debye-Scherrer formula for all peaks and the average crystal size was 97 nm.

The XRD pattern and the Debye-Scherrer equation clearly show that the size of crystal depends on several factors such as intensity, peak expansion, resolution, dislocation density and especially the strain in the material. Strain (ϵ) is calculated using Eq. (2)

$$\epsilon = \frac{\beta_{hkl}}{4\tan\theta} \quad (\text{Eq. 2})$$

In this regard, crystal size and strain are also analyzed using the Williamson-Hall(W-H) model [21-23]. The Williamson-Hall model is used to analyze the relationship between crystal size and pressure.

Depending on the different positions of θ , strain analysis is performed using the Williamson-Hall method. The following results are the addition of the Debye-Scherrer equation and strain parameter (Eq. 3 and 4).

$$\beta_{hkl} = \beta_s + \beta_D \quad (\text{Eq. 3})$$

$$\beta_{hkl} = \left(\frac{k\lambda}{D\cos\theta}\right) + 4\epsilon\tan\theta \quad (\text{Eq. 4})$$

where, β_s is due to the contribution of crystallite size, β_D is due to the strain induced broadening, and β_{hkl} is the half maximum intensity of instrumental corrected broadening. Rearranging Eq. (5) gives:

$$\beta_{hkl}\cos\theta = \left(\frac{k\lambda}{D}\right) + 4\epsilon\sin\theta \quad (\text{Eq. 5})$$

The Eq. (5) is known as W-H equation [21-23] and this is called the uniform deformation model (UDM). Here Eq. (5) stands for UDM where it is assumed that strain is uniform in all crystallographic directions. In Fig. 4, $\beta_{hkl}\cos\theta$ was plotted with respect to $4\sin\theta$ for α -Fe₂O₃ peaks supported in MOF. The particle size is calculated from the y-track of the installed line.

The particle size obtained by the Debye-Scherrer method ($D=97 \text{ nm}$) is slightly different from the particle size calculated by the Williamson-Hall method ($D=100.98 \text{ nm}$), so it can be concluded that strain has very little effect on the average crystal size ($\epsilon=5.77\times 10^{-5}$).

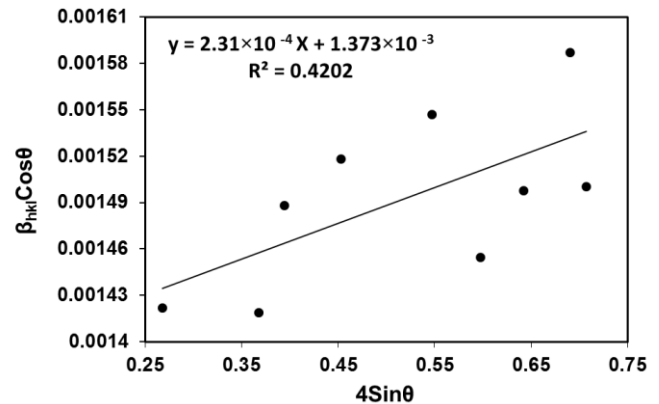


Fig.4. The Plot of $\beta_{hkl} \cos\theta$ vs $4\sin\theta$ for Williamson-Hall (W-H) analysis.

The surface morphology of the synthesized MOF and α -Fe₂O₃/MOF was investigated by SEM images. Fig. (5-A) presents the scanning electron microscope (SEM) images of the synthesized MOF. This image of MOF shows porous and flower-like structures. The morphology of the nanoparticles is like a Dahlia.

The SEM image of α -Fe₂O₃/MOF is shown in Fig. (5-B). This image confirms that the α -Fe₂O₃ structures supported on the MOF are circular and elliptic tears and the size of these particles is less than 100 nm which is consistent with the values obtained from X-ray

diffraction patterns. In this image, it is clear that α -Fe₂O₃ nanoparticles bind to MOF and occupy a large area of

porous and mud-like structure in MOF. This can increase the efficiency of the catalyst.

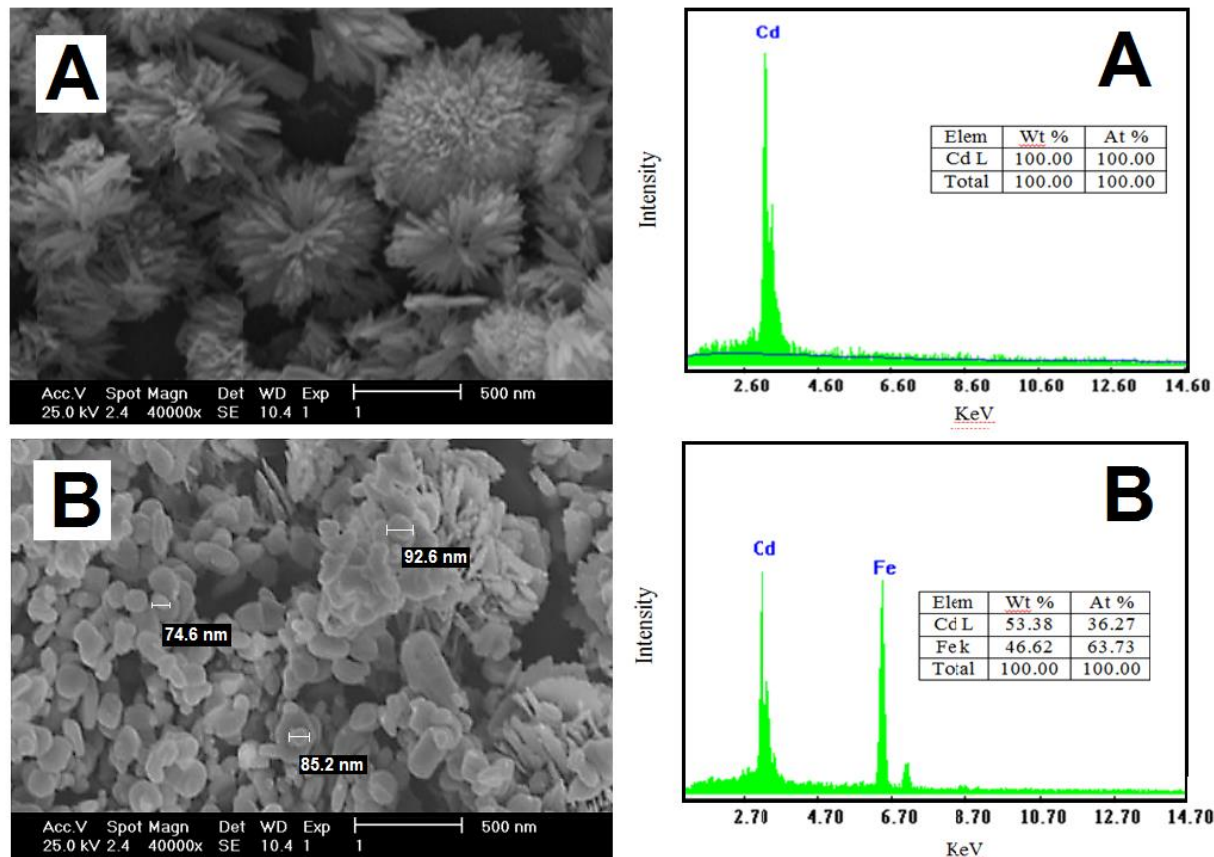


Fig. 5. SEM image and EDX analysis of MOF (A) and α -Fe₂O₃/MOF (B)

EDX analysis is utilized for the elemental composition of specific points in the sample. EDX spectrum for the MOF and α -Fe₂O₃/MOF with a table containing weight and atomic elemental composition percent is shown in **Fig. 5**. According to these analyzes, it can be confirmed that there is no metal impurity in the structure of MOF and α -Fe₂O₃/MOF. Elemental analysis (EDX) for α -Fe₂O₃/MOF (**Fig. 5B**) proves that α -Fe₂O₃ has been present at the sample.

The N₂ adsorption-desorption isotherm of α -Fe₂O₃/MOF and the pore sizes distribution specified by BJH analysis from the N₂ adsorption branch of this isotherm is shown in **Fig. 6**. **Fig. 6** shows that α -Fe₂O₃/MOF isotherm is similar to type IV. At low relative pressure (less than 0.48) the adsorption uptake was relatively small, whereas a steeper increase in the higher relative pressure region ($P/P_0=0.48-1.0$) was observed. It could be considered as an indication of pronounced capillary condensation in the mesoporous. When P/P_0 is checked in the range 0.45-1.0, a small residual loop is

observed in the isotherm, indicating the presence of low porous pores and narrow pores on the sample [24].

Some textural properties of the samples are given in **Table 2**. As shown in **Table 2**, the average pore diameter is approximately 4 nm and these materials were mesoporous. The pore volume and BET surface area of α -Fe₂O₃/MOF were higher than the amount of MOF, but the pore diameters have decreased. Therefore, α -Fe₂O₃ is fixed on the edges of the pores. These results are consistent with the images obtained from SEM. It can be derived that the addition of α -Fe₂O₃ on the MOF had a great effect on the structure of MOF, greatly increasing the surface area, which was suitable cause for improving the photocatalytic efficiency.

To specify the thermal stability, thermogravimetric analysis (TGA) was used. TGA analysis is carried out to study the systematic weight loss and subsequent transformations during heat treatment of the annealed sample. Thermography data for the synthesized catalyst, is presented in **Fig. 7**. It can be seen from **Fig. 7** that as the temperature increases, MOF and α -Fe₂O₃/MOF gra-

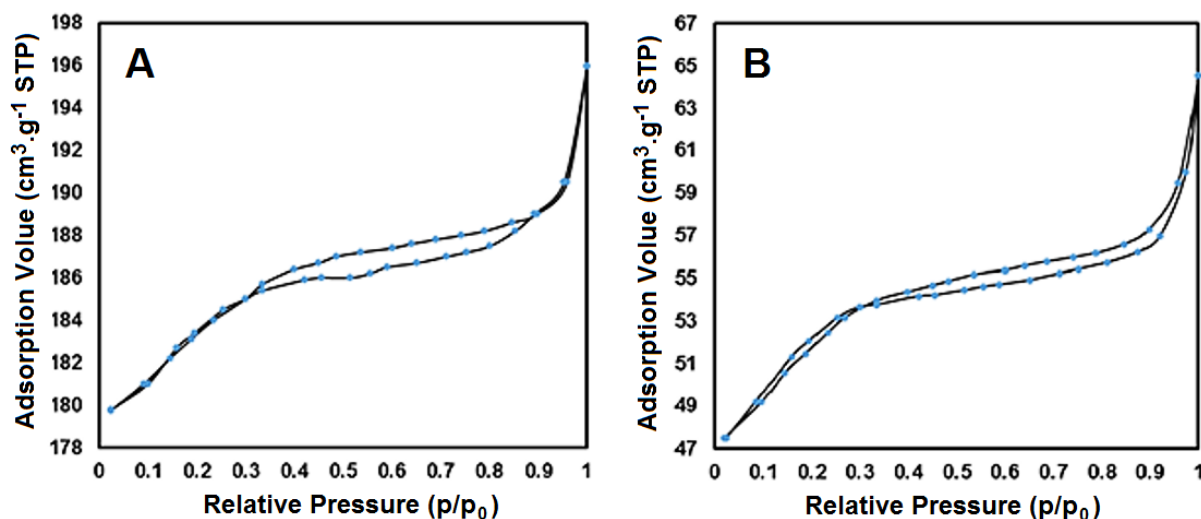


Fig. 6. N₂ adsorption-desorption of α-Fe₂O₃ (A) and α-Fe₂O₃/MOF (B)

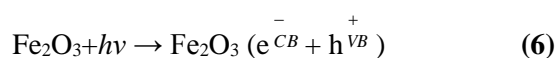
Table 2. Textural properties of MOF and α-Fe₂O₃/MOF. (S_{BET}: BET surface area, V_{total}: Total pore volume, D: Average pore diameter calculated using BJH method)

Sample	S _{BET} (m ² g ⁻¹)	V _{total} (cm ³ g ⁻¹)	D(nm)
MOF	126	0.0892	4.13
α-Fe ₂ O ₃ /MOF	479	0.3245	3.86

-dually lose weight. At 16 to 242 °C, the loss of guest molecule including absorbed water and crystalline water was done from α-Fe₂O₃/MOF and at 200 °C, the loss of these guest molecules from MOF was carried out. At 461 °C and 512 °C about 50% weight loss has been observed in these temperatures, the gradual collapse of the structure of MOF and α-Fe₂O₃/MOF has begun respectively. These results show that α-Fe₂O₃ is loaded into the MOF structure or dispersed in the pores of the MOF and thus the thermal stability of the α-Fe₂O₃/MOF has increased.

3.3. Photocatalytic mechanism and UV/Vis Spectrophotometry analysis of CFZ

The mechanism of photocatalytic reactions by α-Fe₂O₃ is similar to other semiconductors (Fig. 8). This is due to the fact that when α-Fe₂O₃ is illuminated with the light of λ < 390 nm, electrons are promoted from the valence band to the conduction band of the semi conducting oxide to give electron-hole pairs as follows (reactions 6-9) [22-24]:



The valence band (h^{VB}) potential is positive enough to generate hydroxyl radicals as follows:

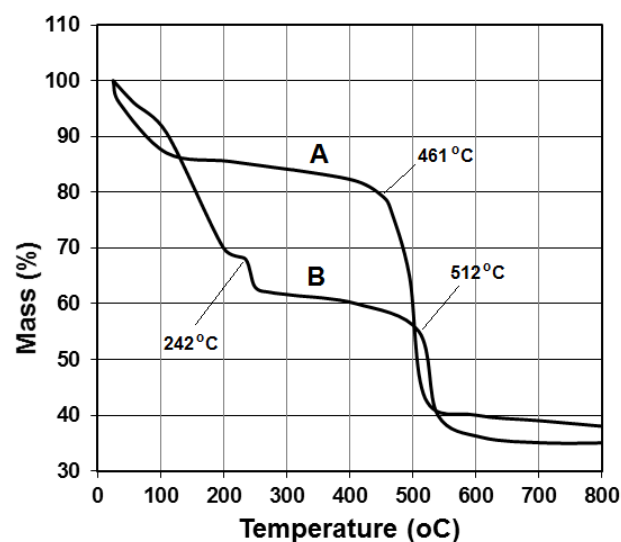
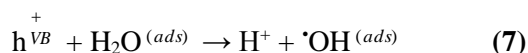
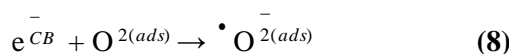


Fig. 7. TGA of MOF (A) and α-Fe₂O₃/MOF (B)



The conduction band (e^{CB}) potential is negative enough to reduce molecular oxygen ($\cdot\text{O}_2^{(ads)}$).



Superoxide radical ions can react with water to form hydroxyl radicals. The hydroxyl radicals and superoxide radical ions are the powerful oxidizing agents and attack CFZ molecules present at or near the surface of Fe₂O₃ as follows:

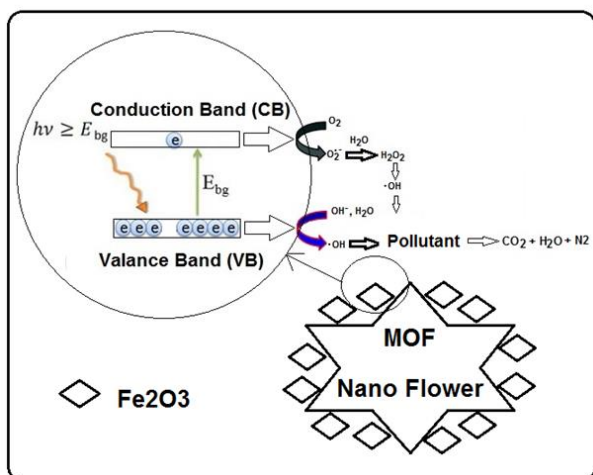
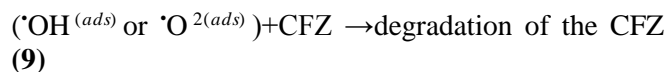


Fig. 8. Schematic of photocatalytic mechanism for decomposition of pollutant in water

Changes of the UV-Vis spectrum in the CFZ photocatalytic decomposition process in the aqueous solution shown in **Fig 9**. Degradation percentage was obtained with the **Eq. (6)**:

$$\text{Degradation percentile } X \% = \frac{A_0 - A_t}{A_0} \times 100 \quad (\text{Eq. 6})$$

Where A_0 and A_t are the absorbance values (in the $\lambda_{\text{max}}=270\text{nm}$) of the solution at 0 and t min after irradiation, respectively.

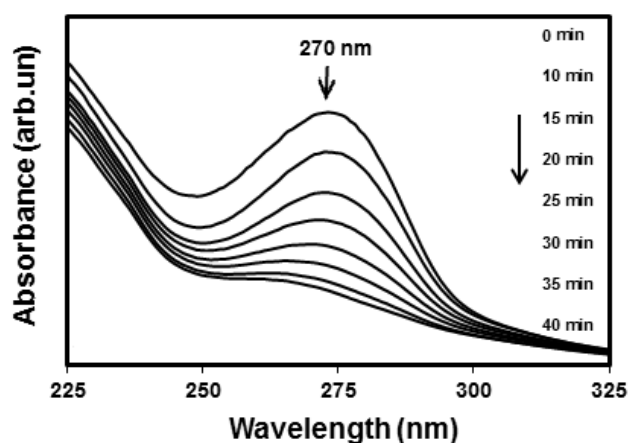


Fig. 9. Absorption changes of UV-Vis in CFZ photocatalytic decomposition (CFZ initial concentration = 30 ppm, $\alpha\text{-Fe}_2\text{O}_3/\text{MOF}$ amount = 150 $\text{mg} \cdot \text{l}^{-1}$, H_2O_2 initial concentration = 5 ppm, pH = 4)

Different methods of UV-C effect on CFZ degradation percentiles are shown in **Fig. 10**. This Fig indicates that using UV-C, alone or with H_2O_2 , has no significant effect on CFZ photocatalytic decomposition; however, using some amounts of $\alpha\text{-Fe}_2\text{O}_3/\text{MOF}$ (50 $\text{mg} \cdot \text{l}^{-1}$)

increases degradation percentiles significantly. The highest degradation of CFZ was obtained from the simultaneous application of UV-C, H_2O_2 , MOF and $\alpha\text{-Fe}_2\text{O}_3/\text{MOF}$. The highest efficiency of degradation occurs in the first 10 minutes of irradiation. Best performance is achieved in the first 30 minutes of the test.

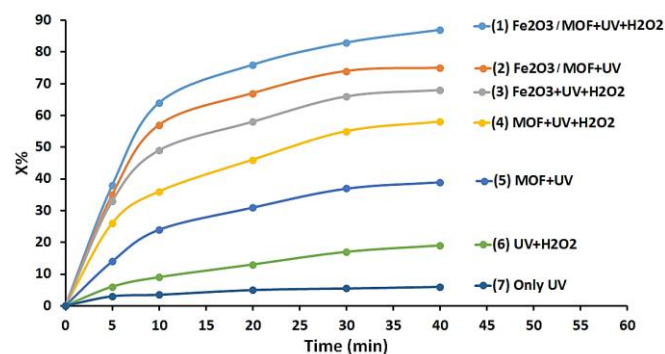


Fig. 10. Analyzing different modes of UV effects on CFZ photocatalytic degradation percentile (CFZ initial concentration = 30 ppm, catalyst amount = 150 $\text{mg} \cdot \text{l}^{-1}$, H_2O_2 initial concentration = 5 ppm, pH = 4)

As shown in **Fig. 10**, hydrogen peroxide has increased catalyst efficiency. The reason is that in the steps of reaction mechanism (**Fig. 2**), hydroxyl radicals are formed from the breakdown of hydrogen peroxide molecules based on the following reaction [22, 23].



Therefore, the catalyst and hydrogen peroxide have a synergistic effect and that increases the efficiency of the catalyst in the photocatalytic removal process of CFZ. [23, 24]

3.3. Factorial Design of the Experiments

Evaluation of effective variables including $\alpha\text{-Fe}_2\text{O}_3 / \text{MOF}$ value, initial CFZ concentration, H_2O_2 initial pH and pH is necessary for optimizing the photocatalytic processes. These factors are not independent; therefore single factor analysis will be a long, incomplete and complex process. The modeling using a factorial design method provides a detailed analysis. Saving time and requiring fewer trials to optimize the process are the advantages of this method.

This method can also specify the interaction of variables. Analysis of variance (ANOVA) was used for data analysis. Variance indicates the distribution of data onto the mean. An increase in variance indicates an increase in distribution. [25-27]. Experimental conditions and CFZ degradation percentile for the photocatalytic process based on the full factorial designs method are given in **Table 3**.

Table 3. Experimental conditions and CFZ degradation percentile for photocatalytic process

Experiment No.	CFZ initial Con.(ppm)	Catalyst amount. (mg.l ⁻¹)	H ₂ O ₂ initial Con.(ppm)	pH	Degradation percentile(%)
1	30	150	1	4	64.15
2	70	150	5	8	70.35
3	70	50	5	4	85.88
4	70	150	1	4	69.35
5	30	150	5	4	60.60
6	70	50	1	8	78.21
7	70	50	1	4	83.12
8	70	150	1	8	62.67
9	50	100	3	6	72.47
10	70	150	5	4	71.85
11	30	50	5	4	72.78
12	50	100	3	6	72.46
13	30	50	1	8	75.76
14	30	150	1	8	61.85
15	30	150	5	8	64.32
16	50	100	3	6	72.47
17	30	50	1	4	75.34
18	30	50	5	8	78.37
19	70	50	5	8	85.75

The statistical model of sample data was evaluated by a regression analysis method. The mathematical model is as the **Eq. (7)**:

$$X\% = 72.5395 + 3.4069 A - 6.9106 B + 1.2469 C - 0.3306 D - 0.4944 AB + 1.3756 AC - 1.2594 AD - 0.1094 BC - 0.5144 BD + 1.3531 CD \quad (\text{Eq. 7})$$

where in A, B, C, D are α -Fe₂O₃/MOF amounts, initial concentration of CFZ, initial concentration of H₂O₂, and pH value respectively.

The regression coefficient and the corresponding T and P value are shown in **Table 4**. Positive coefficients have a synergistic effect on the response and negative coefficients have an antagonist effect on the response value. The results show that among the variables affecting the process, the initial concentration of CFZ and pH has an antagonist effect on the response. As specified by these results, the interaction of variables, namely the catalyst amount and the H₂O₂ initial concentration (Catalyst \times H₂O₂) H₂O₂ initial concentration and pH (H₂O₂ \times pH) have positive effects. The other interactions of the variables were negative.

The p-value indicates the probability of error in accepting the validity of the observed results. In this study a p-value of 0.05 indicates with a 5% probability, the relationship we observed in the sample is

coincidental. Therefore, variables with p values less than 0.05 are acceptable in the model.

Analysis of variance (ANOVA) is a type of statistical hypothesis test and this method is based on a set of statistical models that are widely used in the analysis of experimental results [26]. ANOVA was applied to graphically analyze the experimental data to recognize the interaction between process variables and response [26, 27]. The accuracy of the polynomial model was determined according to the coefficient of determination R² and its statistical significance was assessed by the Fisher test (F test). Model terms were evaluated by the probability value (P-value).

The ANOVA results are depicted in **Table 5**. In this Table, the number of parameters that can be changed in the process was shown with the degrees of freedom. The "Adjusted R²" of 99.95 is in reasonable agreement with the "Predicted R²" of 99.82 indicating too, a good predictability of the model.

The Fisher's test was used to evaluate the significance of a model. The Model F-value of 3953.12 implies the model is significant. This model explains perfectly the experimental range studied, as can be seen from the comparison of the graphical representation of actual vs predicted values (**Fig. 11**). **Fig. 11** shows the plot of predicted response by the model versus experimental responses and the R² value. The R² value means an

Table 4. Estimated regression coefficients and corresponding t and p value.

Term	Coefficients	T-Value	P-Value	F-Value
Constant	72.5395	1922.14	0.000	3953.12
Catalyst	3.4069	82.84	0.000	6862.78
CFZ	-6.9106	-168.04	0.000	28237.25
H ₂ O ₂	1.2469	30.32	0.000	919.25
pH	-0.3306	-8.04	0.000	64.63
Catalyst×CFZ	-0.4944	-12.02	0.000	574.55
Catalyst×H ₂ O ₂	1.3756	33.45	0.000	144.51
Catalyst×pH	-1.2594	-30.62	0.000	1118.89
CFZ× H ₂ O ₂	-0.1094	-2.66	0.029	937.77
CFZ×pH	-0.5144	-12.51	0.000	7.07
H ₂ O ₂ ×pH	1.3531	32.90	0.000	156.44

Table 5. Variance analysis (ANOVA) of CFZ photocatalytic decomposition

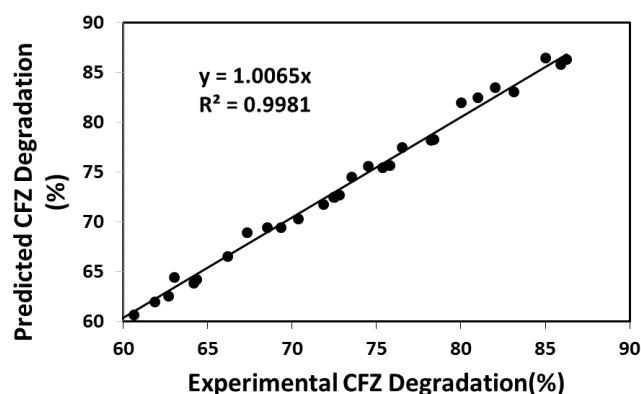
Response	Source	Degree of freedom	Sum of square	Mean square	F
CFZ degradation	Regression	10	1069.73	106.973	3953.12
	Residual error	8	0.22	0.027	
	Total	18	1069.94		

$R^2_{pre}=99.98, R^2_{adj}=99.95$

acceptable agreement between the experimental and predicted values of the fitted data. High correlation and high value of determination coefficient ($R^2= 0.9981$) show the validity of the model.

The residual analysis of full factorial modeling for CFZ photocatalytic degradation process is shown in **Fig. 12**. In the natural probability diagram of distribution processes (**Fig. 12 (a)**), the points around the diagonal straight line indicate the natural distribution of residual values. In **Fig. 12 (b)**, there are seven dots below and eleven dots above the zero line that confirm the random distribution of the residual values [27]. Repeatability and occurrence rates are represented in **Fig. 12 (c)**. If the F value of an experimental parameter is higher than the theoretical value, or the P-value is less than 0.05, this

parameter can affect the test results. The residual plots of each experiment are shown in **Fig. 12(d)**.

**Fig.11.** the plot of predicted response by the model versus experimental responses

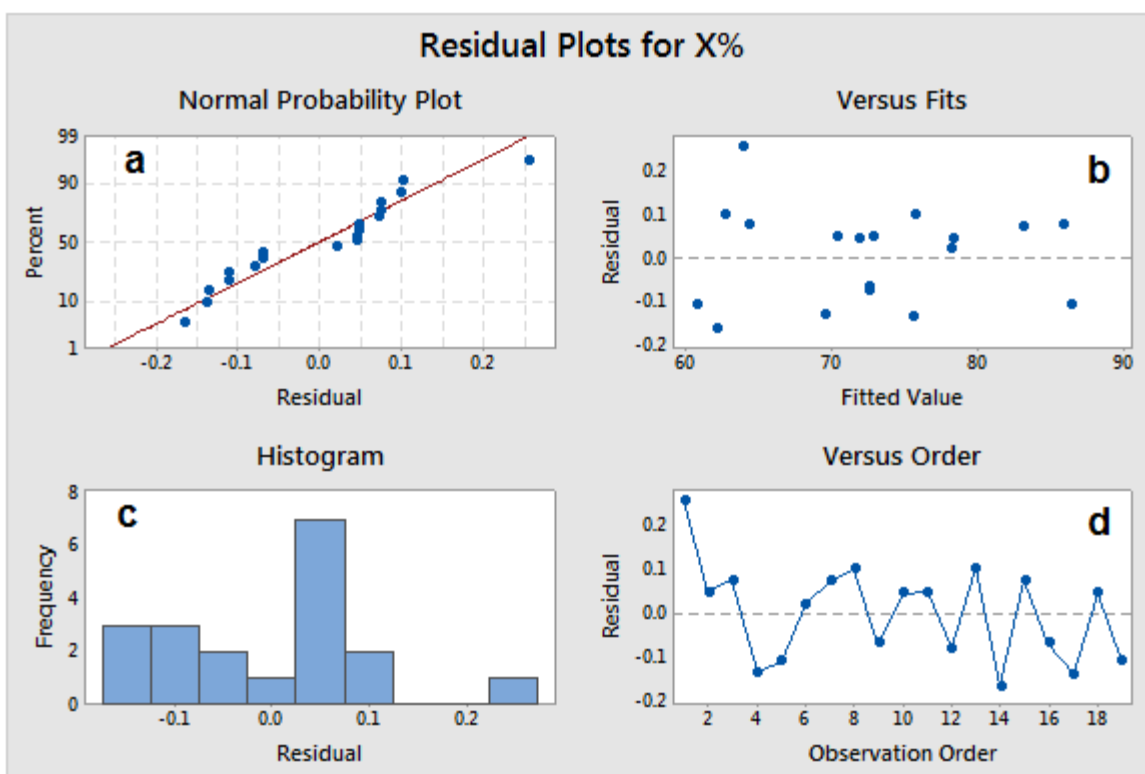
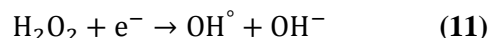


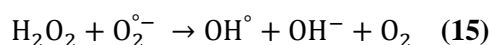
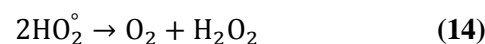
Fig. 12. Residual plots for CFZ photocatalytic degradation percentiles, (a) normal probability plot, (b) residual distribution dispersion coefficient versus efficient values, (c) repeatability and occurrence rate, (d) residual plots of each test

The Pareto chart was used (Fig. 13) to compare the standard effects of different variables in the modeling process and includes the analysis of the main variables and their interactions on the CFZ degradation in aqueous solution [28]. In Fig. 14, the plots of the main effects are shown. By ignoring the interactions, it can be deduced that the initial concentration of CFZ has the most influence on the degradation process. The degradation percentile was significantly increased with increasing α -Fe₂O₃/MOF amount. With the increase of α -Fe₂O₃/MOF photocatalysts, OH radical production increases. After CFZ concentration, catalyst amount affects significantly the photocatalytic degradation processes. So that with an increase in catalyst amount, photocatalytic degradation increases as well. H₂O₂ concentration and pH are the next levels of influence on the photocatalytic degradation of CFZ. If these variables increase, degradation will increase. The addition of hydrogen peroxide to the mixture in photocatalytic processes often results in increased degradation of the pollutants. A number of researchers conducted similar studies and concluded that H₂O₂ has a significant role in antibiotic oxidation [27]. In other words, H₂O₂ is an important agent of advanced oxidation and has great influence on the rate of chemical reactions. Photolysis of hydrogen peroxide as a strong oxidant increases the efficiency of decomposition processes due to the production of hydroxide radicals. In addition, the above

studies show that H₂O₂ is used at different concentrations based on the chemical structures of the pollutants and the different properties of the water matrix. To preserve the efficiency of added H₂O₂, its concentration should be selected in accordance with the type and concentration of the pollutant. In the following reaction, hydrogen peroxide absorbs a photo-electron from the semiconductor bond to produce the hydroxide radical (reaction 11) [27].



pH affects absorption capacity, decomposition of the targeted compound, electric charge distribution on photocatalyst surfaces, and oxidation potential of the band [29,30]. The efficiency of this process in the acidic pH can be explained by the following (reactions 12-15): [29, 30].



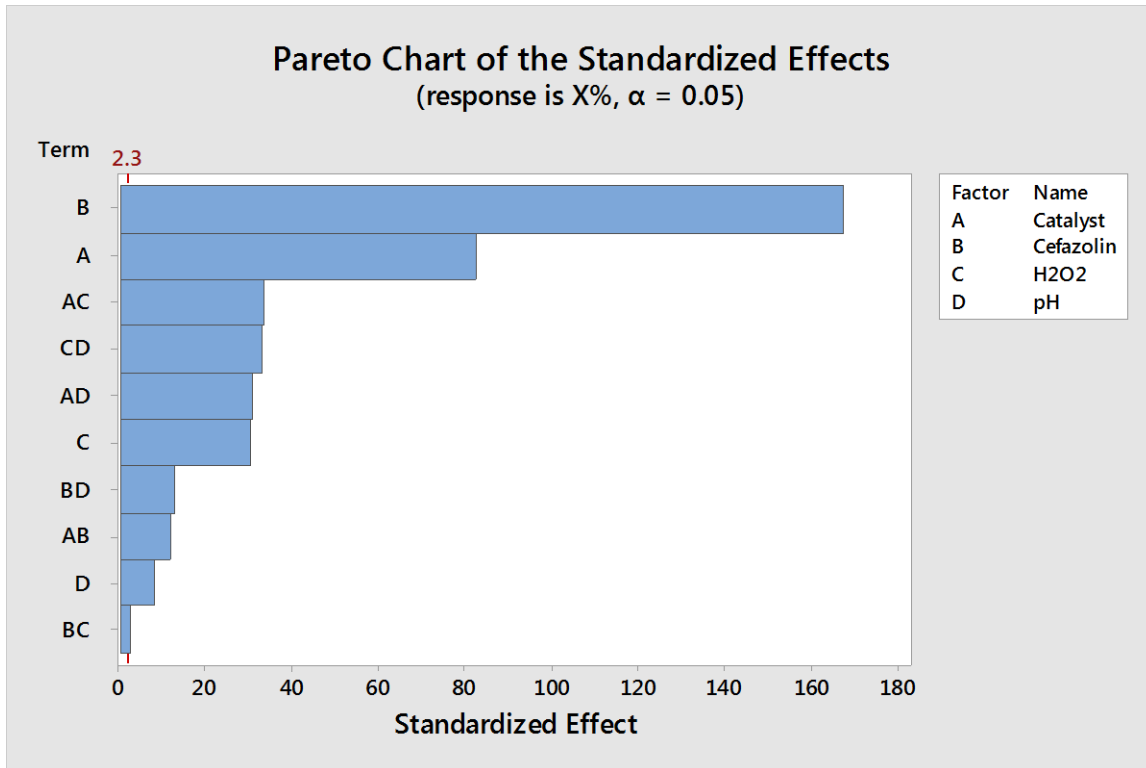


Fig. 13. Pareto Chart of standardization effects for photocatalytic decomposition of CFZ

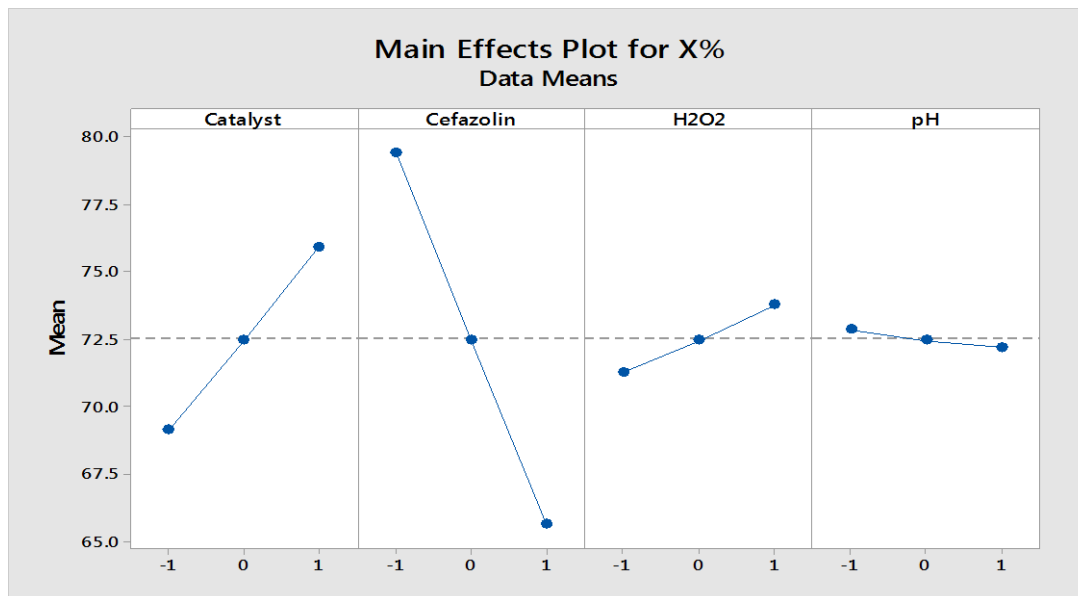


Fig. 14. Analyzing the effects of main variables on CFZ photocatalytic degradation percentiles

3.4. Kinetic of Photocatalytic Degradation of CFZ

The $\ln(A_0/A)$ was plotted versus reaction time for CFZ photocatalytic decomposition in the optimum condition (Fig. 15). The linearity of this graph indicates that the reaction kinetic is pseudo-first-order with a rate coefficient of $k=0.0752 \text{ min}^{-1}$.

The kinetics of heterogeneous photocatalytic processes is often described by the Langmuir–Hinshelwood kinetic model (Eq. 8) [31-34].

$$r = -\frac{dC}{dt} = \frac{k_r K_e C}{1 + K_e C} \quad (\text{Eq. 8})$$

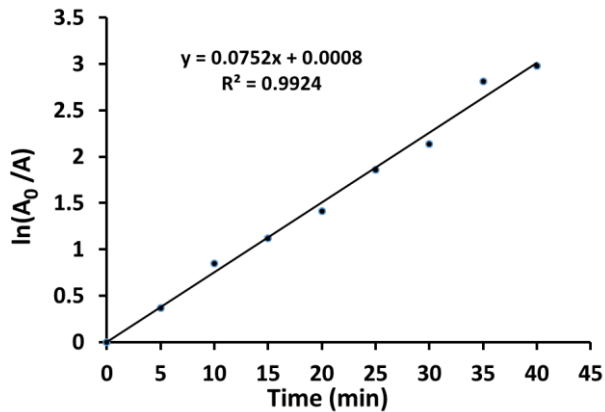


Fig. 15. Kinetic plot of $\ln(A_0/A)$ versus irradiation time for CFZ photocatalytic degradation (Initial concentration of CFZ = 30 ppm, $\alpha\text{-Fe}_2\text{O}_3/\text{MOF}$ = 150 mg. l⁻¹, Initial concentration of H₂O₂ = 5 ppm, pH = 4)

where r is the reaction rate, C is the concentration of CFZ, k_r and K_e are the apparent reaction rate constant and the apparent equilibrium of adsorption constant, respectively. By replacing r with the initial reaction rate r_0 and C_0 with the initial concentration of CFZ in the raw effluents, **Eq. (9)** can be written in the following linearized form:

$$\frac{1}{r_0} = \frac{1}{k_r K_e C_0} + \frac{1}{k_r} \quad (\text{Eq. 9})$$

To determine the values of k_r and K_e using the initial rate method, a series of experiments were carried out with varying initial concentration of CFZ. **Fig. 16** shows the plot of $(1/r_0)$ against $(1/C_0)$ with very high correlation coefficient ($R^2=0.9939$). The calculated values of k_r and K_e were 66.225 mg l⁻¹ min⁻¹ and 0.0011 mg⁻¹, respectively. The CFZ adsorption is the controlling step of the photocatalytic process because the value of k_r is substantially higher than that of K_e .

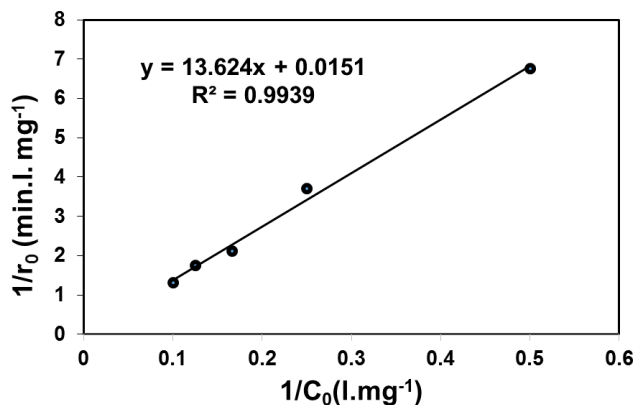


Fig. 16: Langmuir-Hinshelwood kinetics plot for photocatalytic removal of CFZ using Fe₂O₃/MOF. ($\alpha\text{-Fe}_2\text{O}_3/\text{MOF}$ = 150 mg. l⁻¹, Initial concentration of H₂O₂ = 5 ppm, pH = 4)

To reuse the photocatalyst, the test is repeated five times in optimum condition (CFZ initial concentration = 30 ppm, catalyst amount = 150 mg. l⁻¹, H₂O₂ initial concentration = 5 ppm, pH = 4). The results of removal efficiency were $X_1=85.88\%$, $X_2=85.85\%$, $X_3=85.83\%$, $X_4=85.78\%$ and $X_5=85.75\%$ respectively. These results confirm reuse capability of $\alpha\text{-Fe}_2\text{O}_3$ /MOF photocatalyst.

The organic content of the wastewater sample can be estimated by chemical oxygen demand (COD) and Total organic carbon (TOC). The amount of COD evaluates equal of oxygen for the oxidation of organic matter in the sample by the K₂Cr₂O₇ as a strong oxidant, the Ag₂SO₄ as a catalyst and H₂SO₄ as a powerful acidic condition. HgSO₄ is also used to eliminate chloride interference in reaction with dichromate [35, 36].

Total Organic Carbon (TOC) is a measure of the total amount of carbon in organic compounds in pure water and aqueous systems such as waste water. The TOC is important because it is a general indicator for easy measurement of the approximate level of organic pollution. TOC is determined by thermal thermochemical oxidation and a chemical oxidant, usually a persulfate. Therefore, decrease in COD and TOC confirms the mineralization of CFZ into mineral ions, CO₂, H₂O and other nutrients. The results obtained from the spectrum show a higher removal percentage compared to the COD and TOC results because these spectra only show the breakdown of CFZ molecules and CFZ molecules are first converted into smaller molecules and in a few steps; they will be completely converted to mineral compounds.

To confirm the CFZ mineralization in the photocatalytic process, the amount of TOC and COD were measured under optimum conditions. The decrease percentage of TOC and COD obtained was 67% and 78%, respectively under optimum condition after 40-minute irradiation, therefore CFZ molecules were decomposed in solutions and effectively mineralized.

Previous research on the elimination of CFZ by photocatalytic method is summarized in **Table 6**. Due to the different conditions of the process in these studies, it is difficult to compare their results with each other. According to the results, the greatest percentage of CFZ removal was obtained using Ag₃PO₄/BiOBr photocatalyst [37]. It should be noted that in addition to the high cost of Ag₃PO₄/BiOBr, the energy consumption in this procedure (400 watts) is higher than all other processes.

The use of N-doped TiO₂ shows a reduction of 79%, but the catalyst amount (2g/l) was higher than that of other

studies. The use of titanium dioxide and TiO₂ stabilized on the glass surface after two hours has taken the degradation efficiency of 44% and 74%, respectively, which is less efficient than other processes [38].

The use of activated carbon (AC)+ZnO catalyst has given similar results with this catalyst in the presence of CeO₂ in the photocatalytic elimination of CFZ [39]. The AC+ZnO shows a great percentage of removal (about 96%).

The photodegradation of CFZ was investigated in the presence of suspended and immobilized TiO₂ on a glass plate [40]. According to the results of this research, the rate of the photodegradation of the CFZ in the presence of TiO₂ suspension was higher than that in the immobilized TiO₂. However, the removal of CFZ using

these catalysts was less than the removal of this substance using α -Fe₂O₃ /MOF catalysts.

In a study using (AC +ZnO) + CeO₂ as a photocatalyst to remove the antibiotic CFZ, it was found that 96% of the removal of this substance from the aqueous solution was achieved under optimal conditions [41]. It is more expensive than α -Fe₂O₃ /MOF photocatalyst.

According to the above explanation, the preparation of α -Fe₂O₃ /MOF photo-catalyst is relatively simple and inexpensive and has a high stability in aqueous solution. Also, it has a good degradation efficiency (85.88% after 40 min) in the photocatalytic degradation of CFZ aqueous solution.

Table 6. Previous research on the elimination of CFZ by photocatalytic method

Photocatalyst	Condition	Degradation efficiency	References
Ag ₃ PO ₄ /BiOBr	In the Xujiang Electromechanical Plant (XPA)photo-reactor, Irradiation source: a 400 W metal halogen lamp, pH=6.25, amount of photocatalyst: 0.75 g/l, initial CFZ concentrations: 15 mg/l.	100% after 30 min	[37]
N-doped TiO ₂	In batch-type photo-reactor, Irradiation source: 5×8 W backlights fluorescent lamps emitting light between 300 and 400 nm with a maximum at 365 nm, pH=6.4, amount of photocatalyst: 2 g/l, initial CFZ concentrations:0.02 mol/l.	79.69% after 30 min	[38]
AC+ZnO	In discontinuous photochemical chamber (Batch Reactor), Irradiation source: low-pressure mercury lamp with the power of 55 watts, pH=3, amount of photocatalyst: 0.1 g/l, initial CFZ concentrations:100 mg/l.	95% after 60 min	[39]
suspended TiO ₂ and immobilized TiO ₂ on a glass plate	In the photoreactor was a borosilicate petri dish (diameter = 12 cm, height = 2.5 cm), Irradiation source: UV lamp (15 W, λ_{\max} = 254 nm, Philips), pH=5, amount of photocatalyst: 500 mg/l, initial CFZ concentrations:20 mg/l.	44.83% after 2 h TiO ₂ on a glass plate 77.58% after 2h in suspended TiO ₂	[40]
(AC +ZnO)+ CeO ₂	In batch photo-reactor, Irradiation source: low-pressure mercury lamp with the power of 55 watts, pH=3, amount of photocatalyst: 0.1 mg/l, initial CFZ concentrations:100 mg/l.	96%	[41]

4. Conclusions

The results indicated that the metal-organic framework can be synthesized using Cadmium nitrate and Terephthalic acid. The structure of this framework was confirmed by XRD, FTIR and EXD experiments, their morphology can be identified by SEM images. High surface areas, regular pores and cluster structure of MOF make it a suitable base for α -Fe₂O₃ Nanophotocatalyst. The α -Fe₂O₃ nanoparticles (supported on the MOF) are interconnected and occupy more surface area on the crystalline surfaces of MOF, which enhances the efficiency of the photocatalytic degradation processes. Combining α -Fe₂O₃ photocatalyst nanoparticles with MOF plays an important role in enhancing the speed and the efficiency of CFZ photocatalytic degradation processes. SSD is a suitable method for supporting of α -Fe₂O₃ on the MOF. Statistical analysis of the results confirmed the reliability and validity of this model. In the absence of interaction of variables, the initial concentration of CFZ and H₂O₂ has positive effects, and α -Fe₂O₃/MOF concentration and pH have negative effects on CFZ degradation. The interaction of variables is very important and should be considered to optimize the degradation percentile. Finally, it is recommended to use this catalyst to remove other organic pollutants in water by a photocatalytic method.

Acknowledgements

Authors preserve their utmost gratitude for Islamic Azad University of Arak for experimental supports.

References

- [1] H. Vera, S. Lúcia, J. Environ. Manage. 92 (2011) 2304-2347.
- [2] F. Yuan, C. Hu, X. Hu, J. Qu, M. Yang, Water. Res. 43 (2009) 1766-1774.
- [3] I. A. Balcioglu, M. Otker, Chemosphere. 50(1) (2003) 85-95.
- [4] M. B Heeb, J. Criquet, S. G. Zimmermann-Steffens, Water. Res. 48 (2014) 15-42.
- [5] N. Omrani, A. Nezamzadeh-Ejhieh, J. Water. Proc. Eng. 33 (2020) 101094-101105.
- [6] A. Pourtaheri, S. Jiao, S. Zheng, D. Yin, L. Wang, L. Chen, Chemosphere. 73 (2008) 377-382.
- [7] H. Derikvandi, A. Nezamzadeh-Ejhieh, J. Hazard. Mater. 321 (2017) 629-638
- [8] A. Nezamzadeh-Ejhieh, Chem. Eng. Res. Des. 104 (2015) 835-843.
- [9] M. Mishra, D. M. Chun, Appl. Catal. A: Gen. 498 (2015) 126-141
- [10] A. Norouzi, A. Nezamzadeh-Ejhieh, Physica B: Condensed Matter. 599 (2020) 412422-412431.
- [11] M. Zebardast, A. F. Shojaei, K. Tabatabaeian, Iran. J. Catal. 8 (4) (2018) 297-309
- [12] M.H. Yap, K. L. Fow, G.Z. Chen, Green. Energ. Environ. 2 (2017) 218-245.
- [13] J. Long, S. Wang, Z. Ding, S. Wang, Y. Zhou, L. Huang, X. Wang, Chem. Commun. 48 (2012) 11656-11658.
- [14] N. E. Fard, R. Fazaeli, Iranian J. Catal. 8(2) (2018) 133-141
- [15] S. Ghattavi, A. Nezamzadeh-Ejhieh, Inter. J. Hydrog. Energy. 45 (2020) 24636-24656
- [16] S. Bharathi, D. Nataraj, D. Mangalaraj, Y. Masuda, K. Senthil, K. Yong, J. Phys. D: Appl. Phys. 43 (2010) 015501-015510.
- [17] A. Nezamzadeh-Ejhieh, A. Shirzadi, Chemosphere. 107 (2014) 136-144
- [18] B. Alqasem, N. Yahya, S. Qureshi, M. Irfan, Z. U. Rehman, H. Soleimani, Mat. Sci. Eng. B. 217 (2017) 49-62
- [19] A. Nezamzadeh-Ejhieh, Z. Ghanbari-Mobarakeh, J. Ind. Eng. Chem. 21 (2015) 668-676
- [20] M.B. Bahar Khodadadi, Iran. J. Catal. 6(1) (2016) 37-42
- [21] S. D. Khairnar, V. S. Shrivastava, Iran. J. Catal. 8 (2018) 143-150
- [22] M. Balakrishnan, R. John, Iran. J. Catal. 10(1) (2020) 1-16
- [23] Y. T. Prabhu, K. V. Rao, V. S. S. Kumar, B. S. Kumari, World. J. Nano Sci. Eng. 4 (2014) 21-28.
- [24] A. Kusior, K. Michalec, P. Jelen, M. Radecka, Appl. Surf. Sci. 476 (2019) 342-352
- [25] T. Tamiji, A. Nezamzadeh-Ejhieh, J. Electroanal. Chem. 829 (2018) 95-105
- [26] S. A. Hosseini, R. Saeedi, Iran. J. Catal. 7(1) (2017) 37-46
- [27] M. Saghi, K. Mahanpoor, Int. J. Ind. Chem. 8 (2017) 297-313
- [28] H. Derikvandi, A. Nezamzadeh-Ejhieh, J. Photochem. Photobiol. A: Chem. 348 (2017) 68-78
- [29] R. Dagherir, P. Drogui, M.A.E. Khakani, Electrochim. Acta. 83 (2012) 113-124.
- [30] R. A. French, A. R. Jacobson, B. Kim, S. L. Isley, R. L. Penn, P. C. Baveye, Environ Sci. Technol. 43(5) (2009) 1354-1359.
- [31] B. Divband, A. Jodaei, M. Khatmian, Iran. J. Catal. 9 (2019) 63-70
- [32] Z. Shams-Ghahfarokhi, A. Nezamzadeh-Ejhieh, Mater. Sci. Semicond. Proc. 39 (2015) 265-275.
- [33] S. D. Khairnar, M. R. Patil, V. S. Shrivastava, Iran. J. Catal. 8(2) (2018) 143-150
- [34] N. Omrani, A. Nezamzadeh-Ejhieh, J. Photochem. Photobiol. A: Chem. 400 (2020) 112726-112735.
- [35] M. Mehrali-Afjani, A. Nezamzadeh-Ejhieh, H. Aghaei, Chem. Phys. Lett. 759 (2020) 137873-137882.
- [36] Y. Xiao, X. Song, Z. Liu, R. Li, X. Zhao, Y. Huang, J. Ind. Eng. Chem. 45 (2017) 248-256.
- [37] Y.Y. Gurkan, N. Turkten, A. Hatipoglu, Z. Cinar, Chem. Eng. J. 184 (2012) 113-124.
- [38] M.R. Samarghandi, A. Rahmani, G. Asgari, G. Ahmadidoost, A. Dargahi, Global. NEST. J. 20 (2018) 399-407.
- [39] M. Shokri, G. Isapour, M. A. Behnajady, S. Dorosti, Desalin. Water. Treat. 57(27) (2016) 12874-12881.
- [40] M. R. Samarghandi, A. Dargahi, A. Rahmani, G. Asgari, G. Ahmadidoost, J Environ Health Eng. 5(2) (2018) 132-146.